Spatial metabolomics principles and application to cancer research

Mélanie Planque[1,2*], Sebastian Igelmann[1,2*], Ana Margarida Ferreira Campos[1,2*], Sarah-Maria Fendt[1,2]

[1] Laboratory of Cellular Metabolism and Metabolic Regulation, VIB-KU Leuven Center for Cancer Biology, VIB, Leuven, Belgium

[2] Laboratory of Cellular Metabolism and Metabolic Regulation, Department of Oncology, KU Leuven and Leuven Cancer Institute (LKI), Leuven, Belgium

Corresponding author: sarah-maria.fendt@kuleuven.be

*equal contribution

Abstract

Mass spectrometry imaging (MSI) is an emerging technology in cancer metabolomics. Desorption Electrospray Ionization (DESI) and Matrix Assisted Laser Desorption Ionization (MALDI) MSI are complementary techniques to identify hundreds of metabolites in space with close to single cell resolution. This technology leap enables research focusing on tumor heterogeneity, cancer cell plasticity and the communication signals between cancer and stromal cells in the tumor microenvironment (TME). Currently, unprecedented knowledge is generated using spatial metabolomics in fundamental cancer research. Yet, also translational applications are emerging, including the assessment of spatial drug distribution in organs and tumors. Moreover, clinical research investigates the use of spatial metabolomics as a rapid pathology tool during cancer surgeries. Here, we summarize MSI applications, the knowledge gained by this technology in space, future directions and developments needed.

Highlights

- Identification and quantification of metabolites by mass spectrometry imaging
- Infusion of ^{13}C labeled stable isotopes: challenges and achievements
- MALDI- and DESI-MSI in metabolomics cancer research
- Using MSI for translational and clinical applications

Keywords

Metabolomics, Mass spectrometry imaging, Metabolite identification, Cancer research, Labelled isotope tracing, Tumor heterogeneity, cancer cell plasticity, tumor microenvironment (TME)

Introduction

Metabolic rewiring is an important modulator of cancer progression [1,2] which may contribute to treatment resistance [3] highlighting the need for assessing metabolites and metabolic conversion rates. Bulk metabolite analysis by mass spectrometry (MS) combined with chromatographic methods has been the state-of-the-art method to analyze metabolites in cancer research. Metabolites are extracted from biofluids, cells or tissues, yielding information on the average metabolite concentration in the sample. However, deeper knowledge on the spatial distribution and architecture of metabolism within the tumor tissues is lost [4].

Mass spectrometry imaging (MSI) is a label-free technique that allows spatial mapping of hundreds of metabolites and drugs directly from a tissue section [5]. It allows to assess tumor heterogeneity, cancer cell plasticity and cancer-stromal cell communication in the tumor microenvironment (TME). It may provide improved diagnosis, understanding of pathologies, and antitumor drug distributions in the organs [6].

Here, we focus on the application of matrix assisted laser desorption ionization (MALDI) and desorption electrospray ionization (DESI) MSI in cancer research by highlighting recent advances and remaining challenges.

1. MALDI- and DESI-MSI for metabolomics analysis

1.1 Matrix Assisted Laser Desorption Ionization (MALDI)

MALDI-MSI allows spatial visualization of metabolites and in particular lipids in tissues using laser ionization [7]. A matrix is applied directly on tissue sections, forming co-crystals with metabolites [8]. Upon radiation with the laser beam, the matrix is ionized (addition or loss of a proton) and charges are transferred to the metabolites, resulting in their desorption and ionization [8,9] (Figure 1, Table 1). The choice of the matrix

determines the acquisition mode (negative or positive), and the ionization efficiency of the different metabolites [10]. The number of detected metabolites varies depending on matrix spraying, instrument parameters, and stability of the metabolites. Factors such as number of matrix layers, matrix solvents, flow rates and temperature, as well as number of laser shots per pixel, laser intensity and frequency influence metabolite detection. Therefore, matrix and MSI settings need to be optimized based on the nature of the metabolites and/or lipids for optimal detection [11–20]. For example, N-(1-naphthyl) ethylene dihydrochloride (NEDC) matrix was selected for negative mode MALDI-MSI due to its low signal interference and highest metabolite coverage when compared to 9-aminoacridine (9-AA) and 1,5-Diaminonaphthalene (1,5-DAN) [11], while the flow rate of matrix deposition increased as the number of layers increased [14].

1.2 Desorption Electrospray Ionization DESI

DESI-MSI uses electrospray ionization whereby a fine spray of charged solvent droplets extracts metabolites from tissues [21] (Table 2, Figure 1). DESI-MSI, like MALDI-MSI, is a soft ionization technique with the added advantage that matrix ablation is largely absent, allowing to analyze the same tissue section several times with different ionization modes, spatial resolutions or to perform MS/MS for metabolite confirmation. Therefore, high-speed data acquisition at lower resolution can be used to select specific regions for analysis with high spatial resolution. The lack of matrix, which often interferes with a mass-to-charge ratio (m/z) lower than 500 Da, makes DESI-MSI particularly suited for the measurement of small metabolites [22–31]. For example, measuring small metabolite by DESI-MSI was used to distinguish with nearly 90% accuracy between normal and cancerous human prostate tissue [22]. Similarly, fatty acid, TCA cycle metabolite and phospholipid concentrations were different between normal and cancerous prostate tissue [23], while invasive breast cancers were distinguished from adjacent benign tissue by concentration differences in saturated lipids and antioxidant molecules, and molecular subtypes of breast cancer were classified by lipid profiles [27].

1.3 Comparison of DESI- and MALDI-MSI in metabolomics

The use of DESI- and MALDI-MSI differs depending on the metabolites of interest (Tables 1 and 2) and the application purpose. DESI-MSI is faster in sample preparation and has the possibility of direct tissues analysis at atmospheric pressure [32]. Moreover, tissues can be processed for histological staining directly after DESI-MSI [26], and the lack of a matrix allows the measurement of small molecules (e.g. lactate, glucose, amino acids). In contrast, the spatial resolution of MALDI-MSI is currently better (Tables 1 and 2) because of the high precision of the laser (< 5 µm). The introduction of the nano-DESI improved spatial resolution for DESI-MSI to 10 µm [33]. While this spatial resolution is close to single cell resolution [34], true single cell analysis is still one of the main

challenges. Also, metabolite delocalization or/and difficulties in sample preparation of friable tissues (loss of structural structure of the tissue) [35] remain obstacles in MSI approaches.

In summary, MALDI- and DESI-MSI are complementary approaches. While MALDI-MSI presents a higher spatial resolution, DESI-MSI is better suited for lower mass metabolites. Therefore, the choice between MALDI- and DESI-MSI depends on the biological question.

2. Advances in DESI- and MALDI-MSI in metabolomics

2.1 Identification and quantification of metabolites

Metabolite detection includes signal normalization, raw data visualization for each metabolite (images and MS spectra), mass alignment (on-line calibration during data acquisition) and molecular annotation with libraries. Thereby software like SCiLS Lab and High Definition Imaging coupled to libraries such as MetaboScape, Metaspace or Progenesis QI are important tools [36,37]. Notably, the material used to embed the tissues and the MALDI matrices can interfere with metabolites detection [38] and needs to be imaged as negative control.

Identification and detection of metabolites in the low mass range is challenging because of the high number of isomers, and matrix clusters in the case of MALDI-MSI. Fourier Transform (FT) ion cyclotron resonance (ICR) [11] and Orbitrap [12,15] mass spectrometers were introduced in the field due to their high resolving power and mass accuracy. However, FTICR and Orbitrap require tandem MS to distinguish between isomers and employ long scan times, resulting in longer time of analysis [39]. Recently, it was demonstrated that trapped ion mobility spectrometry (TIMS), can accurately distinguish metabolites peaks from matrix peaks and separate isomeric metabolites [39]. In TIMS ions elute based on their mobility, which is determined by the mass, charge and size of the ion.

Additional metabolite identification approaches are on-tissue chemical derivatization (OTCD), on-tissue spiking of the target metabolites or tandem measurements. OTCD can identify amino acids, among other metabolites and increases the ionization of a metabolite by adding a charge to the metabolite or a more prone to ionization moiety. The resulting higher m/z value avoids interferences coming from matrix clusters. Fluoromethylpyridinium-based reactive matrices that selectively target phenolic and

primary amine groups were used to map low-abundant neurotransmitters in the brain [40]. However, OTCD limits considerably the list of target metabolites. Additionally, on-tissue spiking of the target metabolites predicted possible formation of abundant adducts with hydrogen, sodium, potassium or chloride ions arising from inorganic salts or residual water [38,41]. Another commonly used approach to confirm peak identification is on-tissue tandem measurements (MS/MS). However, some metabolites (e.g. amino acids, lactate, and pyruvate) result in too small fragments to perform tandem measurements. By consequence, liquid chromatography (LC)-MS and gas chromatography (GC)-MS are widely used to confirm metabolite identification within the same bulk sample exploiting chromatographic metabolite separation [12].

Most DESI- and MALDI-MSI data are relative. One of the bigger limitations for absolute quantification is the change in desorption/ionization efficiencies between sample regions. On-tissue spotting of a serial dilution of standards directly onto or below a control tissue section (dilution series strategy), and/or the use of mimetic tissue models, are possible solutions to achieve absolute quantification [42]. The latter are homogenized tissues, which simulate the ion suppression caused by endogenous competing molecules of the actual sample, spiked with metabolite standards [43,44]. Using the series dilution strategy, Lan C. et al., quantified 2-hydroxyglutarate (2-HG) in glioma samples [45]. Liver sections were used as control tissue and spotted with a serious dilution of 2-HG and subsequently coated with a NEDC matrix containing ^{13}C labeled 2-HG disodium salt (internal standard). The peak area of 2-HG of each calibration spot from the liver was normalized against the peak area of ^{13}C labeled 2-HG and plotted against the corresponding concentration resulting in a standard curve that allowed absolute 2-HG quantification in the glioma sections from patients coated with the same ^{13}C 2-HG containing matrix [45]. Classically, mimetic tissue models require longer sample preparation times, but new developments have largely overcome this drawback [46]. Comparing the mimetic tissue model and the dilution series strategy it was found that mimetic tissue models correct better for tissue-specific ion suppression effects and extraction efficiencies [47,48].

2.2 Labelled enrichment of stable isotopes

Stable non-radioactive isotopes (^{13}C, ^{2}H or ^{15}N) can also be used to estimate the contribution of nutrients and metabolic pathways to the observed metabolic changes [49]. The use of labelled nutrients to infer spatial metabolic pathway activity has not been standardized. Nonetheless, tissue samples from mammals infused with ^{13}C-labelled nutrients have been analyzed [11,12,14,50]. Using MALDI-MSI in kidney sections from isotope-labeled infused mice, it was found that glutamine and citrate are the most used nutrients in the cortex, while in the medulla there is a preference for fatty acids [11].

Additionally, it was found that ^{13}C-glucose incorporation into lipids was higher in breast cancer-derived brain metastases then in noncancerous brain tissue [12].

However, the lack of chromatographic separation and matrix cluster effects, add additional complexity to ^{13}C labeled MSI compared to bulk data [11]. To overcome this challenge, G. Wang et al. traced the spatiotemporal incorporation of ^{13}C isotope into glycolysis and TCA cycle intermediates using two instruments: a Rapiflex MALDI-TOF/TOF system and a high resolution instrument fitted with a MALDI-FTICR-MSI to confirm the labelling distribution [14]. Subsequently, only the m/z features present in both datasets and with similar tissue distributions, were further used to identify the lipid species.

3. Mass spectrometry imaging can be used for fundamental research and clinical applications

3.1 Insights gained into the heterogeneity of tumor metabolism by MSI

MSI has been used to infer the spatial complexity of tumors (Figure 2). In glioblastoma-derived xenografts, an inverse abundance of ATP and acylcarnitine was detected [51]. Resected human brain tissue slices showed differences in antioxidant metabolites, nucleotides and fatty acid composition of tumors versus peritumor material [52]. Additionally, it was shown that glycogen, a multibranched polysaccharide of glucose which serves as energy storage, displays high intratumor and subtype heterogeny in lung cancer [53]. While glycogen levels were high in cancer cells of lung adenocarcinomas, they were high in stroma and endothelial cells of squamous small cell carcinoma. Similarly, 3D cultured cancer cells, a more physiological *in vitro* model of tumors, showed heterogeneity in glutamate, tyrosine and inosine abundance [54]. Likewise, usage of a stable isotope label, followed by MSI, showed differential usage of glucose and glutamine within a population of *in vitro* cultured proliferating cancer cells. This was recapitulated in cancerous tissues but not in normal proliferating cells [55]. Thus, MSI can help to define metabolic tumor heterogeneity. This may allow to better understand treatment response when integrating cellular heterogeneity with drug distribution heterogeneity.

3.2 Information of metabolic interaction of the tumor with the TME gained by MSI

MSI imaging has been used to infer tumor-stroma interactions and drug distribution (Figure 2). It was recently demonstrated that D-2-HG, an oncometabolite produced by cancer cells with an IDH mutation, can be taken up in tumor microenvironment by $CD8^+$ T cells, altering T-cell metabolism and reducing T-cell cytotoxicity [56]. Using MSI combined with cyclic immunofluorescence demonstrated that tumor areas with high D-2-HG were depleted of cytotoxic T cells, suggesting that D-2-HG reduced T cell proliferation in the TME of human glioblastomas. This finding implies that patients with high or low D-2HG will likely not have the same response to immunotherapy. Furthermore, a recent study showed an accumulation of palmitate containing lipids in lung metastases of mice compared to adjacent tissue using MSI [57]. Using single cell RNA sequencing this study further found that the primary breast tumors secretome instructed lung resident alveolar type 2 cells to increase their palmitate release. This resulted in a nutrient priming of the pre-metastatic niche and thus increased palmitate availability for the arriving cancer cells [57].

MSI data suggest that unequal or insufficient drug distribution within tumors may contribute to treatment failure (Figure 2). It was shown that the receptor tyrosine kinase inhibitor imatinib was not detected in liver metastases, although the adjacent tissue was saturated with the drug [58]. Similarly, while the pancreatic cancer treatment Gemcitabine, and in particular its active metabolites were detected throughout tumors, other small molecules such as the ATR inhibitor (AZD6738) was only detected in the surrounding non-cancerous tissue [59]. Further studies showed the distribution of pioglitazone, a peroxisome proliferator-activated receptor agonist currently in clinical trials for some metastatic cancers, in tumors and surrounding liver tissues over time [60]. Similarly heterogeneous distribution of Paclitaxel was shown in malignant pleural mesothelioma explaining the observed only partial success of treatment [61].

In the future, an integrated analysis of metabolic cancer cell-stroma interactions and how they change tumor aggressiveness including therapy resistance are needed.

3.3 Current clinical application of MSI and future directions

MSI may revolutionize classical histopathology to detect tumor cells and to subclassify tumor types. In tissues from prostate cancer patients undergoing curative surgery, MSI was used to differentiate healthy tissue from cancerous tissue by defining tumor margins based on metabolic markers such as citrate and carnitine levels [19]. Similarly, MSI can provide improved subtyping of non-small cell lung cancers into adenocarcinoma and squamous cell carcinoma. This is of particular interest as treatments differ between these subtypes [17]. Similar approaches have been used for high grade serous ovarian cancer

[62] and renal cell carcinomas [63]. DESI-MSI was also used to visualize tumor margins intraoperatively. Within 3 minutes, the surgeon was able to identify tumor versus non-tumor tissue in glioblastoma patients improving likelihood of complete resection in a timely manner [64]. Similar experimental protocols are currently evaluated or have been established for squamous oral cancer [65], gastric cancer [66] or breast cancer [67]. Lastly, MSI was also used to monitor disease progression and recurrence over time, and it was recently demonstrated that metastatic tissue from breast cancer can be identified using MSI based on specific patterns of N-glycans and high mannose in the tumor tissue [68]. Thus, it can be speculated that MSI will become a routine tool in the clinics that allows to detect malignant cancer cells with high accuracy and speed.

An important future direction is to combine several multi-omics techniques such as spatial transcriptomics or multiplex immunohistochemistry with spatial metabolomics allowing the researchers to obtain information of the metabolic state and the expression/protein profile of the tissue/cells on the same tissue slide [69]. In this respect, Wang et al. focused on normal kidney development by combining spatial metabolomics with multiplex immunofluorescence in one tissue slide [70]. To further accelerate integrated multi-omics approaches, it will be essential to advance compatibility between techniques and develop computational approaches for data exploration and visualization. One example of a computational approach that is currently being developed is the MIAAIM tool [71], which allow multi-omics image integration from different spatial platforms.

Conclusion

MSI is becoming a broadly applicable spatial technology. However, some bottlenecks remain and need to be resolved: The spatial resolution delivered by current instruments do not allow to infer subcellular distribution of metabolites without destruction into elements by X-ray fluorescence and nanoSIMS [72]. Furthermore, the nature of MSI analysis requires simultaneous ablation of all ions from a pixel, which limits the identification of metabolites with similar m/z ratio. Until now MSI is mainly performed as singular spatial analysis, yet to infer biological mechanisms in space the integration with other omics layers ideally on the same tissue section is required. Finally, to enable broad approval for patient care further efforts need to be taken to standardize sample preparation, metabolite detection and identification.

Author contribution

MP, SI, AMFC and S-MF wrote the manuscript. AMFC and SI made the Tables and/or Figures.

Acknowledgments

SI is an EMBO fellow (ALTF 13-2022), and S-MF acknowledges funding from the European Research Council under the ERC Consolidator Grant Agreement n. 771486–MetaRegulation, FWO – Research Projects, KU Leuven, Beug Foundation, Stichting tegen Kanker and Fonds Baillet Latour.

Legends

Figure 1. **Principles of mass spectrometry imaging (MSI).** Schematic representation of the different steps involved in MSI, from sample preparation to MS analysis, including the differences in sample preparation and analysis between MALDI and DESI.

Figure 2. **Application of mass spectrometry imaging (MSI).** Overview on the information gained using mass spectrometry imaging (MSI). MSI can be used to visualize drugs, metabolite distributions within the tumor microenvironment and to evaluate the margins of tumors, with close to single cell resolution. In the panel of drug distribution, the top image shows the distribution of AZD6738 and Gemcitabine (GEM) between pancreatic ductal adenocarcinoma (PDAC) and pancreatic tissue [59] On the middle panel is represents the preferred localization of Paclitaxel (PTX) on the margins of a malignant pleural mesothelioma [61]. On the bottom image the absence of imatinib in liver metastasis is visualized by MSI [58]. On the metabolic interactions panel, gliomas with IDH mutations showed a regional distribution of D-2-HG that inversely correlated with the detection of $CD8^+$ T-cells [56]. For tumor margin detection and subtyping, on the top imaged is represented the localization of different metabolites between tumor and surrounding healthy tissue (NAA - N-acetylaspartate) [19], [57], [64]. The image in the middle shows the difference in glycogen localization between the different subtypes of non-small cell lung cancer (LUAD - lung adenocarcinoma; LUSC – lung squamous cell carcinoma) [53].The bottom image shows the use of MSI to monitor the breast tumor progression, showing an accumulation of glycans in metastasis (METS) in comparison to primary tumor (PT) [68].

Table 1. Overview of the recent MALDI applications for MSI of metabolites both in tumoral and non-tumoral tissues. Detailed description on the used MALDI instrument

for MSI, the chosen spatial resolution in µm, the used matrix, the analyzed tissue and the metabolite families that were identified.

Table 2. Overview of the recent DESI applications for MSI of metabolites both in tumoral and non-tumoral tissues. Detailed description on the used DESI instrument for MSI, the chosen spatial resolution in µm, the analyzed tissue and the metabolite families that were identified.

References

1. Rinaldi G, Pranzini E, Van Elsen J, Broekaert D, Funk CM, Planque M, Doglioni G, Altea-Manzano P, Rossi M, Geldhof V, et al.: **In Vivo Evidence for Serine Biosynthesis-Defined Sensitivity of Lung Metastasis, but Not of Primary Breast Tumors, to mTORC1 Inhibition**. *Mol Cell* 2021, **81**:386-397.e7.
2. Martínez-Reyes I, Chandel NS: **Cancer metabolism: looking forward**. *Nat Rev Cancer* 2021, **21**:669–680.
3. Hanahan D: **Hallmarks of Cancer: New Dimensions**. *Cancer Discov* 2022, **12**:31–46.
4. Salviati E, Sommella E, Campiglia P: **MALDI–mass spectrometry imaging: the metabolomic visualization**. In *Metabolomics Perspectives*. . Elsevier; 2022:535–551. *The authors presents the analytical workflow of MALDI–MSI for polar metabolites and lipids analysis focusing mostly in biomedical and pharmaceutical field.
5. Buchberger AR, DeLaney K, Johnson J, Li L: **Mass Spectrometry Imaging: A Review of Emerging Advancements and Future Insights**. *Anal Chem* 2018, **90**:240–265.
6. Dueñas ME, Lee YJ: **Single-Cell Metabolomics by Mass Spectrometry Imaging**. 2021:69–82.
7. Ruiz-Rodado V, Lita A, Larion M: **Advances in measuring cancer cell metabolism with subcellular resolution**. *Nat Methods* 2022, **19**:1048–1063.
8. Lee PY, Yeoh Y, Omar N, Pung Y-F, Lim LC, Low TY: **Molecular tissue profiling by MALDI imaging: recent progress and applications in cancer research**. *Crit Rev Clin Lab Sci* 2021, **58**:513–529. *In this review, MALDI imaging workflow and applications in various niches of cancer research are described. The authors highlight the remaining challenges and future perspectives in cancer research
9. Wu J, Rong Z, Xiao P, Li Y: **Imaging Method by Matrix-Assisted Laser Desorption/Ionization Mass Spectrometry (MALDI-MS) for Tissue or Tumor: A Mini Review**. *Processes* 2022, **10**:388.
10. Ràfols P, Vilalta D, Torres S, Calavia R, Heijs B, McDonnell LA, Brezmes J, del Castillo E, Yanes O, Ramírez N, et al.: **Assessing the potential of sputtered gold nanolayers in mass spectrometry imaging for metabolomics applications**. *PLoS One* 2018, **13**:e0208908.

11. Wang L, Xing X, Zeng X, Jackson SRE, TeSlaa T, Al-Dalahmah O, Samarah LZ, Goodwin K, Yang L, McReynolds MR, et al.: **Spatially resolved isotope tracing reveals tissue metabolic activity**. *Nat Methods* 2022, **19**:223–230. ** Wang et al., use mass spectrometry imaging coupled with stable isotope labeled nutrients to quantify metabolic activities within organs.
12. Ferraro GB, Ali A, Luengo A, Kodack DP, Deik A, Abbott KL, Bezwada D, Blanc L, Prideaux B, Jin X, et al.: **Fatty acid synthesis is required for breast cancer brain metastasis**. *Nat Cancer* 2021, **2**:414–428. **The authors show that breast tumor metastasis growing in the brain display a higher fatty acid synthesis than breast tumor metastasis growing in extracranial sites due to decreased lipid availability.
13. Stopka SA, van der Reest J, Abdelmoula WM, Ruiz DF, Joshi S, Ringel AE, Haigis MC, Agar NYR: **Spatially resolved characterization of tissue metabolic compartments in fasted and high-fat diet livers**. *PLoS One* 2022, **17**:e0261803.
14. Wang G, Heijs B, Kostidis S, Mahfouz A, Rietjens RGJ, Bijkerk R, Koudijs A, van der Pluijm LAK, van den Berg CW, Dumas SJ, et al.: **Analyzing cell-type-specific dynamics of metabolism in kidney repair**. *Nat Metab* 2022, **4**:1109–1118. ** Wang et al., use a mass spectrometry imaging approach combined with isotope tracing and immunofluorescence staining to identify metabolomic perturbations in specific kidney tissue regions during lesion and recovery.
15. Neumann JM, Niehaus K, Neumann N, Knobloch HC, Bremmer F, Krafft U, Kellner U, Nyirády P, Szarvas T, Bednarz H, et al.: **A new technological approach in diagnostic pathology: mass spectrometry imaging-based metabolomics for biomarker detection in urachal cancer**. *Laboratory Investigation* 2021, **101**:1281–1288.
16. Neumann JM, Freitag H, Hartmann JS, Niehaus K, Galanis M, Griesshammer M, Kellner U, Bednarz H: **Subtyping non-small cell lung cancer by histology-guided spatial metabolomics**. *J Cancer Res Clin Oncol* 2022, **148**:351–360. *Neumann et al., use mass spectrometry imaging metabolomics associated to histology and machine learning algorithms to differentiate between non-small cell lung adenocarcinoma and squamous cell carcinoma.
17. Shen J, Sun N, Zens P, Kunzke T, Buck A, Prade VM, Wang J, Wang Q, Hu R, Feuchtinger A, et al.: **Spatial metabolomics for evaluating response to neoadjuvant therapy in non-small cell lung cancer patients**. *Cancer Commun* 2022, **42**:517–535.
18. Denti V, Andersen MK, Smith A, Bofin AM, Nordborg A, Magni F, Moestue SA, Giampà M: **Reproducible Lipid Alterations in Patient-Derived Breast Cancer Xenograft FFPE Tissue Identified with MALDI MSI for Pre-Clinical and Clinical Application**. *Metabolites* 2021, **11**:577.
19. Andersen MK, Høiem TS, Claes BSR, Balluff B, Martin-Lorenzo M, Richardsen E, Krossa S, Bertilsson H, Heeren RMA, Rye MB, et al.: **Spatial differentiation of metabolism in prostate cancer tissue by MALDI-TOF MSI**. *Cancer Metab* 2021, **9**:9.

20. Denti V, Mahajneh A, Capitoli G, Clerici F, Piga I, Pagani L, Chinello C, Bolognesi MM, Paglia G, Galimberti S, et al.: **Lipidomic Typing of Colorectal Cancer Tissue Containing Tumour-Infiltrating Lymphocytes by MALDI Mass Spectrometry Imaging**. *Metabolites* 2021, **11**:599.
21. Arentz G, Mittal P, Zhang C, Ho Y-Y, Briggs M, Winderbaum L, Hoffmann MK, Hoffmann P: **Applications of Mass Spectrometry Imaging to Cancer**. 2017:27–66.
22. Banerjee S, Zare RN, Tibshirani RJ, Kunder CA, Nolley R, Fan R, Brooks JD, Sonn GA: **Diagnosis of prostate cancer by desorption electrospray ionization mass spectrometric imaging of small metabolites and lipids**. *Proceedings of the National Academy of Sciences* 2017, **114**:3334–3339. *The authors use DESI-MSI approach to measure several metabolites and distinguish between cancerous and normal prostate tissue.
23. Morse N, Jamaspishvili T, Simon D, Patel PG, Ren KYM, Wang J, Oleschuk R, Kaufmann M, Gooding RJ, Berman DM: **Reliable identification of prostate cancer using mass spectrometry metabolomic imaging in needle core biopsies**. *Laboratory Investigation* 2019, **99**:1561–1571. *Morse et al. used a mass spectrometry based approach to establish an accurate metabolic profile of prostate cancer.
24. Zhang J, Li SQ, Lin JQ, Yu W, Eberlin LS: **Mass Spectrometry Imaging Enables Discrimination of Renal Oncocytoma from Renal Cell Cancer Subtypes and Normal Kidney Tissues**. *Cancer Res* 2020, **80**:689–698.
25. Vijayalakshmi K, Shankar V, Bain RM, Nolley R, Sonn GA, Kao C, Zhao H, Tibshirani R, Zare RN, Brooks JD: **Identification of diagnostic metabolic signatures in clear cell renal cell carcinoma using mass spectrometry imaging**. *Int J Cancer* 2020, **147**:256–265.
26. Theriault RL, Kaufmann M, Ren KYM, Varma S, Ellis RE: **Metabolomics patterns of breast cancer tumors using mass spectrometry imaging**. *Int J Comput Assist Radiol Surg* 2021, **16**:1089–1099. *The authors apply mass spectrometry imaging to excised breast tumors to distinguish between malignant and benign tissue.
27. Santoro AL, Drummond RD, Silva IT, Ferreira SS, Juliano L, Vendramini PH, Lemos MB da C, Eberlin MN, Andrade VP: ***In Situ* DESI-MSI Lipidomic Profiles of Breast Cancer Molecular Subtypes and Precursor Lesions**. *Cancer Res* 2020, **80**:1246–1257. *Santoro et al. used MSI to distinguish different subtypes of breast cancer based on the identified metabolic profile.
28. Vaughn A, DeHoog RJ, Eberlin LS, Appling DR: **Metabotype analysis of Mthfd1l-null mouse embryos using desorption electrospray ionization mass spectrometry imaging**. *Anal Bioanal Chem* 2021, **413**:3573–3582.
29. León M, Ferreira CR, Eberlin LS, Jarmusch AK, Pirro V, Rodrigues ACB, Favaron PO, Miglino MA, Cooks RG: **Metabolites and Lipids Associated with Fetal Swine Anatomy via Desorption Electrospray Ionization – Mass Spectrometry Imaging**. *Sci Rep* 2019, **9**:7247.

30. Zhang G, Zhang J, DeHoog RJ, Pennathur S, Anderton CR, Venkatachalam MA, Alexandrov T, Eberlin LS, Sharma K: **DESI-MSI and METASPACE indicates lipid abnormalities and altered mitochondrial membrane components in diabetic renal proximal tubules**. *Metabolomics* 2020, **16**:11.
31. Silva AApR, Cardoso MR, Rezende LM, Lin JQ, Guimaraes F, Silva GRP, Murgu M, Priolli DG, Eberlin MN, Tata A, et al.: **Multiplatform Investigation of Plasma and Tissue Lipid Signatures of Breast Cancer Using Mass Spectrometry Tools**. *Int J Mol Sci* 2020, **21**:3611.
32. Banerjee S, Wong AC-Y, Yan X, Wu B, Zhao H, Tibshirani RJ, Zare RN, Brooks JD: **Early detection of unilateral ureteral obstruction by desorption electrospray ionization mass spectrometry**. *Sci Rep* 2019, **9**:11007.
33. He MJ, Pu W, Wang X, Zhang W, Tang D, Dai Y: **Comparing DESI-MSI and MALDI-MSI Mediated Spatial Metabolomics and Their Applications in Cancer Studies**. *Front Oncol* 2022, **12**.
34. Neumann EK, Do TD, Comi TJ, Sweedler J V.: **Exploring the Fundamental Structures of Life: Non-Targeted, Chemical Analysis of Single Cells and Subcellular Structures**. *Angewandte Chemie International Edition* 2019, **58**:9348–9364.
35. Dannhorn A, Kazanc E, Ling S, Nikula C, Karali E, Serra MP, Vorng J-L, Inglese P, Maglennon G, Hamm G, et al.: **Universal Sample Preparation Unlocking Multimodal Molecular Tissue Imaging**. *Anal Chem* 2020, **92**:11080–11088.
36. Nguyen DD, Saharuka V, Kovalev V, Stuart L, Del Prete M, Lubowiecka K, De Mot R, Venturi V, Alexandrov T: **Facilitating Imaging Mass Spectrometry of Microbial Specialized Metabolites with METASPACE**. *Metabolites* 2021, **11**:477. *The authors demonstrate METASPACE to be a useful tool to annotate the chemistry and metabolic exchange factors found in microbial interactions.
37. Alexandrov T, Ovchinnikova K, Palmer A, Kovalev V, Tarasov A, Stuart L, Nigmetzianov R, Fay D, METASPACE contributors K, Gaudin M, et al.: **METASPACE: A community-populated knowledge base of spatial metabolomes in health and disease**. *bioRxiv* 2019, 539478
38. Janda M, Seah BKB, Jakob D, Beckmann J, Geier B, Liebeke M: **Determination of Abundant Metabolite Matrix Adducts Illuminates the Dark Metabolome of MALDI-Mass Spectrometry Imaging Datasets**. *Anal Chem* 2021, **93**:8399–8407.
39. Neumann EK, Migas LG, Allen JL, Caprioli RM, Van de Plas R, Spraggins JM: **Spatial Metabolomics of the Human Kidney using MALDI Trapped Ion Mobility Imaging Mass Spectrometry**. *Anal Chem* 2020, **92**:13084–13091.
40. Shariatgorji M, Nilsson A, Fridjonsdottir E, Vallianatou T, Källback P, Katan L, Sävmarker J, Mantas I, Zhang X, Bezard E, et al.: **Comprehensive mapping of neurotransmitter networks by MALDI–MS imaging**. *Nat Methods* 2019, **16**:1021–1028.
41. Holm NB, Deryabina M, Knudsen CB, Janfelt C: **Tissue distribution and metabolic profiling of cyclosporine (CsA) in mouse and rat investigated by DESI and MALDI**

mass spectrometry imaging (MSI) of whole-body and single organ cryo-sections. *Anal Bioanal Chem* 2022, **414**:7167–7177. **The authors compared DESI- and MALDI-MSI of whole-body and single organ. DESI provided similar results for drug and metabolite distribution in rat jejunum with a slightly better sensitivity.

42. Unsihuay D, Mesa Sanchez D, Laskin J: **Quantitative Mass Spectrometry Imaging of Biological Systems**. *Annu Rev Phys Chem* 2021, **72**:307–329.
43. Lamont L, Hadavi D, Viehmann B, Flinders B, Heeren RMA, Vreeken RJ, Porta Siegel T: **Quantitative mass spectrometry imaging of drugs and metabolites: a multiplatform comparison**. *Anal Bioanal Chem* 2021, **413**:2779–2791.
44. Wu Q: **A review on quantitation-related factors and quantitation strategies in mass spectrometry imaging of small biomolecules**. *Analytical Methods* 2022, **14**:3932–3943.
45. Lan C, Li H, Wang L, Zhang J, Wang X, Zhang R, Yuan X, Wu T, Wu J, Lu M, et al.: **Absolute quantification of 2-hydroxyglutarate on tissue by matrix-assisted laser desorption/ionization mass spectrometry imaging for rapid and precise identification of isocitrate dehydrogenase mutations in human glioma**. *Int J Cancer* 2021, **149**:2091–2098.
46. Barry J, Barry JA, Groseclose MR, Fraser DD, Castellino S: **Revised Preparation of a Mimetic Tissue Model for Quantitative Imaging Mass Spectrometry**. *Protoc Exch* 2018, doi:10.1038/protex.2018.104.
47. Barry JA, Ait-Belkacem R, Hardesty WM, Benakli L, Andonian C, Licea-Perez H, Stauber J, Castellino S: **Multicenter Validation Study of Quantitative Imaging Mass Spectrometry**. *Anal Chem* 2019, **91**:6266–6274.
48. Hansen HT, Janfelt C: **Aspects of Quantitation in Mass Spectrometry Imaging Investigated on Cryo-Sections of Spiked Tissue Homogenates**. *Anal Chem* 2016, **88**:11513–11520.
49. Altea-Manzano P, Broekaert D, Duarte JAG, Fernández-García J, Planque M, Fendt S-M: **Analyzing the Metabolism of Metastases in Mice**. 2020:93–118.
50. Fala M, Somai V, Dannhorn A, Hamm G, Gibson K, Couturier D, Hesketh R, Wright AJ, Takats Z, Bunch J, et al.: **Comparison of ^{13}C MRI of hyperpolarized [1-^{13}C]pyruvate and lactate with the corresponding mass spectrometry images in a murine lymphoma model**. *Magn Reson Med* 2021, **85**:3027–3035.
51. Randall EC, Lopez BGC, Peng S, Regan MS, Abdelmoula WM, Basu SS, Santagata S, Yoon H, Haigis MC, Agar JN, et al.: **Localized Metabolomic Gradients in Patient-Derived Xenograft Models of Glioblastoma**. *Cancer Res* 2020, **80**:1258–1267. *The authors identified in glioblastoma multiforme patient-derived xenograph tumors metabolic gradients within the tumor core, the margins and normal brain tissue. Furthermore, they revealed oxidation of fatty acid for energy production is increased at the edges of tumors in comparison to tumor core.

52. Kampa JM, Kellner U, Marsching C, Ramallo Guevara C, Knappe UJ, Sahin M, Giampà M, Niehaus K, Bednarz H: **Glioblastoma multiforme: Metabolic differences to peritumoral tissue and *IDH*-mutated gliomas revealed by mass spectrometry imaging**. *Neuropathology* 2020, **40**:546–558.
53. Young LEA, Conroy LR, Clarke HA, Hawkinson TR, Bolton KE, Sanders WC, Chang JE, Webb MB, Alilain WJ, Vander Kooi CW, et al.: ***In situ* mass spectrometry imaging reveals heterogeneous glycogen stores in human normal and cancerous tissues**. *EMBO Mol Med* 2022, **14**:e16029.
54. Zang Q, Sun C, Chu X, Li L, Gan W, Zhao Z, Song Y, He J, Zhang R, Abliz Z: **Spatially resolved metabolomics combined with multicellular tumor spheroids to discover cancer tissue relevant metabolic signatures**. *Anal Chim Acta* 2021, **1155**:338342.
55. Zhang Y, Guillermier C, De Raedt T, Cox AG, Maertens O, Yimlamai D, Lun M, Whitney A, Maas RL, Goessling W, et al.: **Imaging Mass Spectrometry Reveals Tumor Metabolic Heterogeneity**. *iScience* 2020, **23**:101355.
56. Notarangelo G, Spinelli JB, Perez EM, Baker GJ, Kurmi K, Elia I, Stopka SA, Baquer G, Lin J-R, Golby AJ, et al.: **Oncometabolite d-2HG alters T cell metabolism to impair CD8^{+} T cell function**. *Science (1979)* 2022, **377**:1519–1529. **The authors used MSI to display the impact of lactate and d-2-HG gradients in the tumor microenivornment on T cell function.
57. Altea-Manzano P, Doglioni G, Liu Y, Cuadros AM, Nolan E, Fernández-García J, Wu Q, Planque M, Laue KJ, Cidre-Aranaz F, et al.: **A palmitate-rich metastatic niche enables metastasis growth via p65 acetylation resulting in pro-metastatic NF-κB signaling**. *Nat Cancer* 2023, **4**:344–364. ** Authors used MALDI-MSI to show an accumulation of palmitate and palmitate derivatives in metastatic lesions in the lung.
58. Abu Sammour D, Marsching C, Geisel A, Erich K, Schulz S, Ramallo Guevara C, Rabe J-H, Marx A, Findeisen P, Hohenberger P, et al.: **Quantitative Mass Spectrometry Imaging Reveals Mutation Status-independent Lack of Imatinib in Liver Metastases of Gastrointestinal Stromal Tumors**. *Sci Rep* 2019, **9**:10698. *Authors show absence of imatinib in lliver metasasis tumor tissue showing the use of MSI to evaluate drug treatment efficencies in tumors.
59. Strittmatter N, Richards FM, Race AM, Ling S, Sutton D, Nilsson A, Wallez Y, Barnes J, Maglennon G, Gopinathan A, et al.: **Method To Visualize the Intratumor Distribution and Impact of Gemcitabine in Pancreatic Ductal Adenocarcinoma by Multimodal Imaging**. *Anal Chem* 2022, **94**:1795–1803.
60. Morosi L, Matteo C, Meroni M, Ceruti T, Fuso Nerini I, Bello E, Frapolli R, D'Incalci M, Zucchetti M, Davoli E: **Quantitative measurement of pioglitazone in neoplastic and normal tissues by AP-MALDI mass spectrometry imaging**. *Talanta* 2022, **237**:122918.

61. Giordano S, Morosi L, Veglianese P, Licandro SA, Frapolli R, Zucchetti M, Cappelletti G, Falciola L, Pifferi V, Visentin S, et al.: **3D Mass Spectrometry Imaging Reveals a Very Heterogeneous Drug Distribution in Tumors**. *Sci Rep* 2016, **6**.
62. Kassuhn W, Klein O, Darb-Esfahani S, Lammert H, Handzik S, Taube ET, Schmitt WD, Keunecke C, Horst D, Dreher F, et al.: **Classification of Molecular Subtypes of High-Grade Serous Ovarian Cancer by MALDI-Imaging**. *Cancers 2021, Vol 13, Page 1512* 2021, **13**:1512.
63. Erlmeier F, Sun N, Shen J, Feuchtinger A, Buck A, Prade VM, Kunzke T, Schraml P, Moch H, Autenrieth M, et al.: **MALDI Mass Spectrometry Imaging—Prognostic Pathways and Metabolites for Renal Cell Carcinomas**. *Cancers (Basel)* 2022, **14**:1763.
64. Pirro V, Alfaro CM, Jarmusch AK, Hattab EM, Cohen-Gadol AA, Cooks RG: **Intraoperative assessment of tumor margins during glioma resection by desorption electrospray ionization-mass spectrometry**. *Proceedings of the National Academy of Sciences* 2017, **114**:6700–6705. **Use of MSI for intraoperative margin detection in glioma.
65. Yang X, Song X, Zhang X, Shankar V, Wang S, Yang Y, Chen S, Zhang L, Ni Y, Zare RN, et al.: **In situ DESI-MSI lipidomic profiles of mucosal margin of oral squamous cell carcinoma**. *EBioMedicine* 2021, **70**:103529.
66. Eberlin LS, Tibshirani RJ, Zhang J, Longacre TA, Berry GJ, Bingham DB, Norton JA, Zare RN, Poultsides GA: **Molecular assessment of surgical-resection margins of gastric cancer by mass-spectrometric imaging**. *Proceedings of the National Academy of Sciences* 2014, **111**:2436–2441.
67. Basu SS, Stopka SA, Abdelmoula WM, Randall EC, Gimenez-Cassina Lopez B, Regan MS, Calligaris D, Lu FF, Norton I, Mallory MA, et al.: **Interim clinical trial analysis of intraoperative mass spectrometry for breast cancer surgery**. *NPJ Breast Cancer* 2021, **7**:116. **Clinical trial analysis for the use of MSI intraperatively in breast cancer.
68. Ščupáková K, Adelaja OT, Balluff B, Ayyappan V, Tressler CM, Jenkinson NM, Claes BSR, Bowman AP, Cimino-Mathews AM, White MJ, et al.: **Clinical importance of high-mannose, fucosylated, and complex N-glycans in breast cancer metastasis**. *JCI Insight* 2021, **6**:e146945.
69. Hsieh W-C, Budiarto BR, Wang Y-F, Lin C-Y, Gwo M-C, So DK, Tzeng Y-S, Chen S-Y: **Spatial multi-omics analyses of the tumor immune microenvironment**. *J Biomed Sci* 2022, **29**:96.
70. Wang G, Heijs B, Kostidis S, Rietjens RGJ, Koning M, Yuan L, Tiemeier GL, Mahfouz A, Dumas SJ, Giera M, et al.: **Spatial dynamic metabolomics identifies metabolic cell fate trajectories in human kidney differentiation**. *Cell Stem Cell* 2022, **29**:1580-1593.e7.
71. Hess JM, Ilieş I, Schapiro D, Iskra JJ, Abdelmoula WM, Regan MS, Theocharidis G, Wu CL, Veves A, Agar NYR, et al.: **MIAAIM: Multi-omics image integration and tissue**

state mapping using topological data analysis and cobordism learning. *bioRxiv* 2021, doi:10.1101/2021.12.20.472858.

72. Decelle J, Veronesi G, Gallet B, Stryhanyuk H, Benettoni P, Schmidt M, Tucoulou R, Passarelli M, Bohic S, Clode P, et al.: **Subcellular Chemical Imaging: New Avenues in Cell Biology**. *Trends Cell Biol* 2020, **30**:173–188.

Figure 1

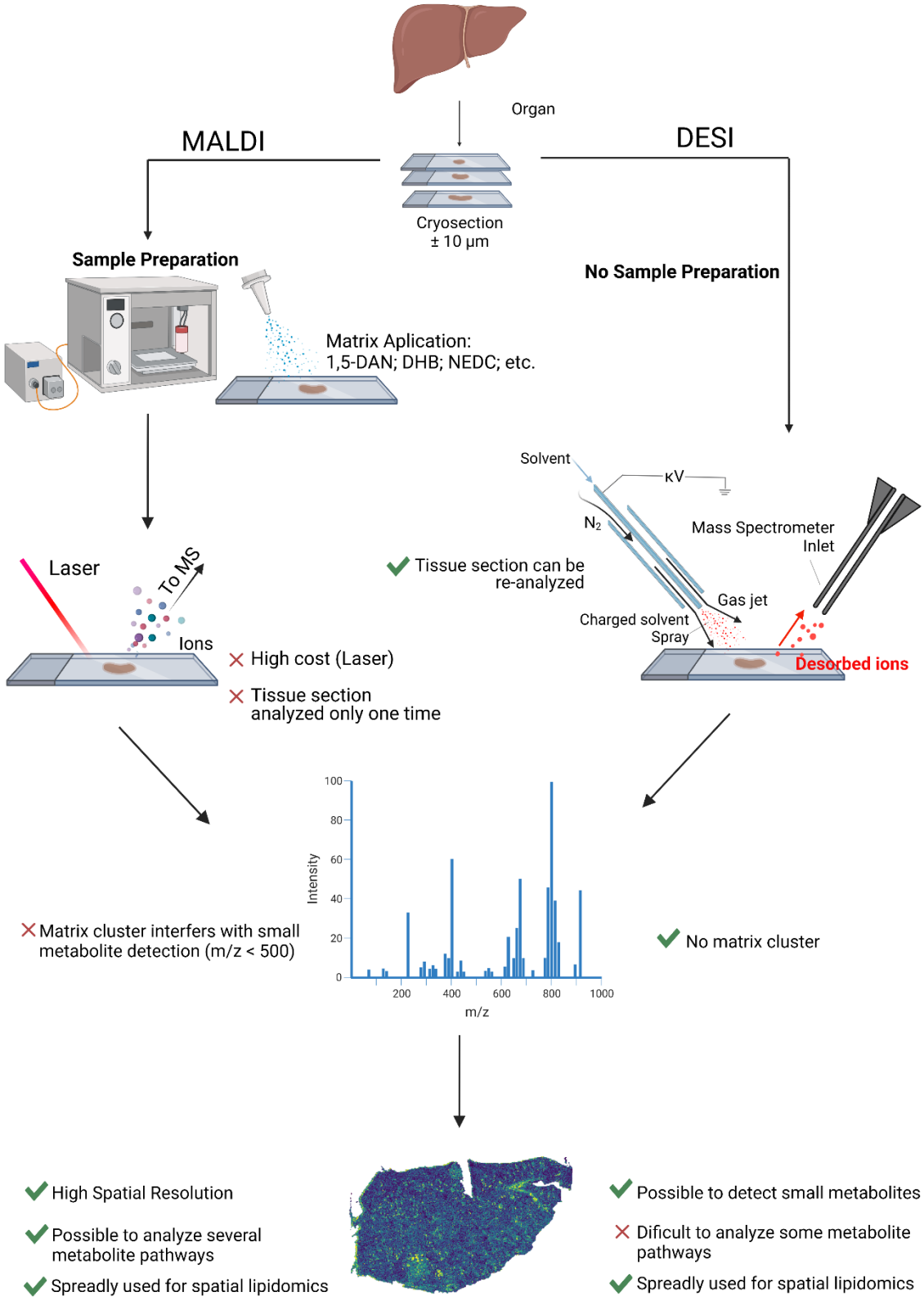
Organ
MALDI
DESI
Cryosection
± 10 µm
Sample Preparation
No Sample Preparation
Matrix Aplication:
1,5-DAN; DHB; NEDC; etc.
Solvent
kV
N2
Mass Spectrometer
Inlet
Gas jet
Charged solvent
Spray
Desorbed ions
Laser
To MS
Ions
Tissue section can be
re-analyzed
High cost (Laser)
Tissue section
analyzed only one time
Intensity
m/z
Matrix cluster interfers with small
metabolite detection (m/z < 500)
No matrix cluster
High Spatial Resolution
Possible to analyze several
metabolite pathways
Spreadly used for spatial lipidomics
Possible to detect small metabolites
Dificult to analyze some metabolite
pathways
Spreadly used for spatial lipidomics

Figure 2:

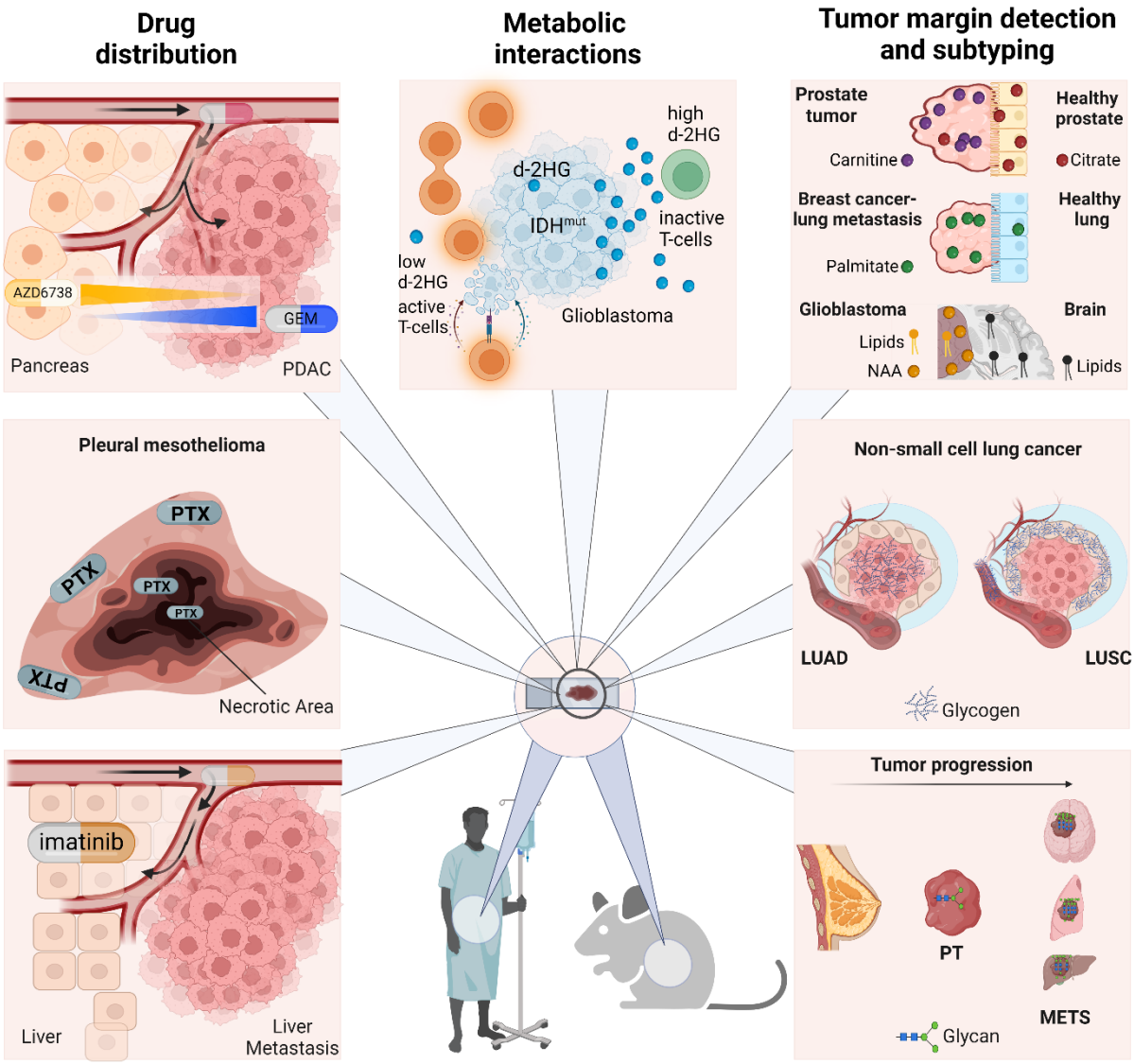
Drug distribution
Metabolic interactions
Tumor margin detection and subtyping
AZD6738
GEM
Pancreas
PDAC
high d-2HG
d-2HG
IDHmut
inactive T-cells
low d-2HG
active T-cells
Glioblastoma
Prostate tumor
Healthy prostate
Carnitine
Citrate
Breast cancer-lung metastasis
Healthy lung
Palmitate
Glioblastoma
Brain
Lipids
NAA
Lipids
Pleural mesothelioma
PTX
Necrotic Area
Non-small cell lung cancer
LUAD
LUSC
Glycogen
imatinib
Liver
Liver Metastasis
Tumor progression
PT
METS
Glycan

Table 1. Overview of the recent MALDI applications for MSI of metabolites both in tumoral and non-tumoral tissues. Detailed description on the used MALDI instrument for MSI, the chosen spatial resolution in µm, the used matrix, the analyzed tissue and the metabolite families that were identified.

MALDI-MSI Instrument	Spatial Resolution (µm)	Matrix	Spray	Metabolites	Tissue/ Type of Cancer	Ref
Autoflex Speed MALDI-TOF/TOF MS	20; 200	4.4 mg/mL 1,5-DAN in hydrochloride acid:ethanol 78:22 (v/v)	TM-Sprayer	4 amino acids; 3 glycolysis intermediates; 4 TCA cycle intermediates; 2 fatty acids; 4 nucleotides; 4 purine pathway intermediates; 1 PE; 1 PS	Renal sections from control and diabetic nephropathy WISTAR rats	(Z. Wang et al. 2021)
MALDI coupled to a solariX XR FT ICR	20 – 50	10mg/mL NEDC in 70:30 methanol:water (v/v)	TM sprayer	5 amino acids; 1 glycolysis intermediate; 2 TCA cycle intermediates; 6 nucleotides	Kidneys and Brains from fasted mice	(L. Wang et al. 2022)
MALDI LTQ Orbitrap XL	Not detailed	5mg/mL 1,5-DAN in acetone:water 70:30 (v/v)	TM-Sprayer	4 fatty acids	Noncancerous mice brain tissue and BT474 tumors growing in the brain of mice	(Ferraro et al. 2021)
rapidfleX MALDI Tissuetyper	30	20 mg/mL DHB in 70% methanol/0.1% trifluoroacetic acid; 7 mg/mL NEDC in 70% methanol.	TM sprayer	5 amino acids; 1 glycolysis intermediate; 1 TCA cycle intermediate; 3 nucleotides; 15 PC; 3 LPC; 11 PE; 7 PS; 5 PI; 1 SM; 1 PG	Human prostate cancer	(Andersen et al. 2021)
timsTOF fleX	30; 50	4.4 mg/mL 1,5- DAN in hydrochloric acid:methanol 1:1 (v/v) solution	TM sprayer	Nucleotides; Glycolysis; Pentose Phosphate Pathway; Fatty Acids	Livers of Fasted and high-fat diet mice	(Stopka et al. 2022)
RapifleX MALDI-TOF/TOF	5	7 mg/mL NEDC in methanol:acetonitrile:deionized water 70:25:5 (v/v/v)	SunCollect Sprayer	3 glycolysis intermediates; 1 TCA Cycle intermediate; 3 amino acids; 1 fatty acid; 1 pentose phosphate pathway intermediate	Mice kidneys	(G. Wang et al. 2022)
rapifleX MALDI Tissuetyper	50	7 mg/mL NEDC in methanol:water 70:30 (v/v)	TM sprayer	2 amino acids	Non-small cell lung cancer	(Neumann et al. 2022)

Spectroglyph MALDI/ESI injector coulpled to Q-Exactive Plus Orbitrap	75	7 mg/mL NEDC in methanol:water 70:30 (v/v)	TM sprayer	1 amino acid; 1 TCA cycle intermediate; 1 PI	Uracal & colorectal adenocarcinomas	(Neumann et al. 2021)
Bruker Solarix 7T FT-ICR MS	50	10 mg/mL 9-aminoacridine hydrochloride monohydrate in 70% methanol	SunCollect Sprayer	PA; LPI; CPA; LPA; PE; SM; PC; LPE; LPC; PGP; TG; PI; Cer; 1 TCA Cycle intermediate; 1 amino acid	Human non-small cell lung cancer	(Shen et al. 2022)
rapifleX MALDI Tissuetyper	50	1 mg/mL CHCA in methanol:water (70:30, v/v) with aniline	HTX M5 Sprayer	1 PI; 2 PA; 2 PG; 5 PE; 1 PS	Xenograft mice tumor from patient-derived breast cancer	(Denti, Andersen, et al. 2021)
MALDI-TOF/TOF ultrafleXtreme	100	30 mg/mL in 50% methanol and 0.2% TFA	ImagePrep	>50 PC; 8 TG; 2 DG; 5 MG; 2 Cer	head and neck squamous cell carcinoma located in tongue	(Bednarczyk et al. 2019)
rapifleX MALDI Tissuetyper	50	10 mg/mL 9-AA was in 70% methanol	HTX TM-Sprayer	3 PA; 1 PE; 1 SM; 3 PS; 9 PI	Colorectal cancer	(Denti, Mahajneh, et al. 2021)

TCA Cycle: Tricarboxylic Acid Cycle; 9-AA: 9-aminoacridine; 1,5-DAN: 1,5-Diaminonaphthalene; CHCA: α-cyano-4-hydroxy-cinnamic acid; DHB: 2,5-dihydroxybenzoic acid; NEDC: N-(1-naphthyl) ethylenediamine dihydrochlorid; PA: phosphatidic acid; LPA: LysoPA; CPA: cyclic PA; PS: phosphatidylserine; PE: phosphatidylethanolamine; LPE: LysoPE; PI: phosphatidylinositol; LPI: LysoPI; PC: phosphatidylcholine; LPC: LysoPC; PG: phosphatidylglycerol; LPG: lysoPG; Cer: ceramide; CL: cardiolipin; PA: phosphatidic acid; SM: sphingomyelin; PGP: phosphatidylglycerophosphate; TG: triacylglycerol; DG: diacylglycerol; MG: monoacylglycerol;

Table 2. Overview of the recent DESI applications for MSI of metabolites both in tumoral and non-tumoral tissues. Detailed description on the used DESI instrument for MSI, the chosen spatial resolution in µm, the analyzed tissue and the metabolite families that were identified.

DESI-MSI Instrument	Spatial Resolution (µm)	Solvent	Flow (µL/min)	Metabolites	Tissue/ Type of Cancer	Ref
2D DESI coupled to Xevo-G2 XS Q-Tof	50	Methanol:water (95:5, v/v) and 50 pg/µL leucine enkephalin	1.5	2 PE; 3 LPE; 3 PI; 2 PC; cholesterol sulfate; 2 fatty acids; 1 TCA cycle intermediate; 1 amino acid;	Prostate tissue	(Morse et al. 2019)
DESI coupled to a hybrid LTQ-Orbitrap Elite	150	DMF:acetonitrile (v/v 1:1)	1.2	13 free fatty acids; 2 amino acids; 1 glycolysis intermediate; >15 CL; 7 PI; 8 PE; 2 LPE; 1 LPE-P; 3 PE-P; 1	Kidney; renal oncocytoma; renal cell carcinoma	(J. Zhang et al. 2020)

				PE-O; 6 PG; 1 PG-P; 1 LPG; 8 PC; 1 LPC; 1 PA; 1 LPA; 10 PS; 1 PS-P; 5 DG; >5 Cer		
DESI coupled to a hybrid LTQ-Orbitrap Elite	200	DMF:acetonitrile (v/v 1:1)	1.0	2 TCA cycle intermediates; 2 glycolysis intermediates; 2 amino acids; 4 fatty acids; 2 PG; 3 PI; 3 PS; 3 PE	renal cell carcinoma	(Vijayalakshmi et al. 2020)
2D DESI-MS coupled to a Xevo-G2 XS TOF	100	Methanol:water (95:5, v/v)	1.5	3 fatty acids	Human female breast cancer	(Theriault et al. 2021)
2D DESI coupled to a Q Exactive HF hybrid quadrupole orbitrap	200	Methanol	1.5	4 DG ; 7 Cer; 7 PE; 7 PG; 10 PS; 1 PA; 8 PI; 1 TG; 12 fatty Acids; 3 aminoacids	Breast tumor	(Santoro et al. 2020)
Q Exactive Orbitrap and Q Exactive HF Orbitrap mass spectrometer fitted with a 2D Omni spray stage and a lab-built DESI sprayer.	100	Acetonitrile:DMF (3:1, v/v)	1.2	33 fatty acids; 4 amino acids; 2 glycolysis intermediates; uracil; adenine	Mouse Embryos	(Vaughn et al. 2021)
2D Omni Spray DESI imaging coupled to a Q-Exactive Orbitrap	200	Acetonitrile:DMF (1:1, v/v)	1.5	7 PS; 3 PE; 5 PI; 2 PC; 4 PG; 1 Cer; 2 CL; 1 PA; 1 TG; 3 PE-O; 1 PS-O; 1 PS-P	Human Breast Cancer	(Silva et al. 2020)
2D Omni Spray DESI imaging coupled to a Q-Exactive Orbitrap	200	Acetonitrile:DMF (1:1, v/v)	1.2	1 amino acid; 7 fatty acids; 3 Cer; 8 PE; 3 PG; 4 PS; 4 PI; 3 CL; Cholesterol-sulfate	Renal cortical sections from mice	(G. Zhang et al. 2020)
DESI spray coupled to LTQ linear ion trap	300	Acetonitrile:DMF (1:1, v/v)	1.5	2 amino acids; 11 fatty acids; 3 Cer; 3 PE; 3 PE-P; 2 PEp; 4 PG; 9 PS; 1 PC; 7 PI; 1 ST	Swine fetuses	(León et al. 2019)

DMF: Dimethylformamide; PS: phosphatidylserine; PS-O: alkyl-PS; PS-P: alkenyl-PS; PE: phosphatidylethanolamine; ; PE-P: alkenyl-PE; PEp: PE phosphate; LPE: lysoPE; LPE-P: alkenyl-LPE; PI: phosphatidylinositol; PC: phosphatidylcholine; LPC: l;ysoPC; PG: phosphatidylglycerol; PG-P: alkenyl-PG; LPG: lysoPG; Cer: ceramide; CL: cardiolipin; PA: phosphatidic acid; LPA: lysoPA; DG: diacylglycerol; TG: triacylglycerol; ST: sulfatide